Before in vivo studies: In vitro screening of sphingomyelin nanosystems using a relevant 3D multicellular pancreatic tumor spheroid model

Nadege Bidan, Sainza Lores, Aure Vanhecke, Valérie Nicolas, Severine Domenichini, Rafael López, María de La Fuente, Simona Mura

Before *in vivo* studies: *in vitro* screening of sphingomyelin nanosystems using a relevant 3D multicellular pancreatic tumor spheroid model

Nadege Bidan[a,‡], Saínza Lores[b,‡], Aure Vanhecke[a], Valérie Nicolas[c], Severine Domenichini[c], Rafael López[d,e], María de la Fuente[b,e,*], Simona Mura[a,*]

[a]Institut Galien Paris-Saclay, UMR 8612, CNRS, Université Paris-Saclay, Faculté de Pharmacie, 5 rue Jean-Baptiste Clément, F92296 Châtenay-Malabry cedex, France

[b]Nano-Oncology and Translational Therapeutics Unit, Health Research Institute of Santiago de Compostela (IDIS), SERGAS, 15706 Santiago de Compostela, Spain

[c]UMS-IPSIT MIPSIT Microscopy facility, Université Paris-Saclay, Inserm, CNRS, Ingénierie et Plateformes au Service de l'Innovation Thérapeutique, 92296, Châtenay-Malabry, France

[d]Translational Medical Oncology group (ONCOMET), Health Research Institute of Santiago de Compostela (IDIS), SERGAS, 15706 Santiago de Compostela, Spain

[e]Biomedical Research Networking Center on Oncology (CIBERONC), Madrid, 28029, Spain

[*]Corresponding author at: Institut Galien Paris-Saclay, UMR 8612, CNRS, Université Paris-Saclay, Faculté de Pharmacie, 5 rue Jean-Baptiste Clément, F92296 Châtenay-Malabry cedex, France;
NanoOncology and Translational Therapeutics Unit, Health Research Institute of Santiago de Compostela (IDIS), SERGAS, 15706 Santiago de Compostela, Spain.
E-mail address: simona.mura@universite-paris-saclay.fr *(S. Mura) and* maria.de.la.fuente.freire@sergas.es *(M. de la Fuente)*

‡ Equal contribution

Abstract

Sphingomyelin nanosystems have already shown to be promising carriers for efficient delivery of anticancer drugs. For further application in the treatment of pancreatic tumor, the investigation on relevant *in vitro* models able to reproduce its physio-pathological complexity, is mandatory. Accordingly, a 3D heterotype spheroid model of pancreatic tumor has been herein constructed to investigate the potential of bare and polyethylene glycol-modified lipids nanosystems in terms of their ability to penetrate the tumor mass and deliver drugs. Regardless of their surface properties, the lipid nanosystems successfully diffused through the spheroid without inducing toxicity, showing a clear safety profile. Loading of the bare nanosystems with a lipid prodrug of gemcitabine was used to evaluate their therapeutic potential. While the nanosystems were more effective than the free drug on 2D cell monocultures, this advantage, despite their efficient penetration capacity, was lost in the 3D tumor model. The latter, being able to mimic the tumor and its microenvironment, was capable to provide a more realistic information on the cell sensitivity to treatments. These results highlight the importance of using appropriate 3D tumour models as tools for proper *in vitro* evaluation of nanomedicine efficacy and their timely optimisation, so as to identify the best candidates for later *in vivo* evaluation.

Keywords: Multicellular 3D tumor spheroids, lipid nanosystems, sphingomyelin, pancreatic cancer, gemcitabine

1. Introduction

Nanoscale drug carriers have been receiving a substantial attention in the recent times as a promising approach to overcome many of the concerns associated to conventional chemotherapies, namely rapid drug metabolism and elimination, and/or a nonspecific distribution accompanied with off-target adverse effects. Overall, these so-called "nanomedicines" are expected to provide increased therapeutic activity and enhance the therapeutic index of the loaded drug (Bor et al., 2019; Tibbitt et al., 2016).

As confirmation of the effectiveness of this strategy, several nanomedicines have already been introduced on the market and several others have reached advanced stage clinical trials (Anselmo and Mitragotri, 2019, 2021; Barenholz, 2012). Noteworthy is that, among them, the majority is made of lipids. The latter are extremely interesting as building blocks due to their biocompatibility and safety profile, both of which are prerequisites for materials chosen for drug delivery applications. Accordingly, a great deal of interest has continued to be devoted to lipid nanoscale systems, leading to the development of a diverse range of carriers such as liposomes, nanoemulsions, solid-lipid nanoparticles, mainly for application in the oncology field (Filipczak et al., 2020; Garcia-Pinel et al., 2019; Kim et al., 2017; Large et al., 2021; Layek et al., 2020; Lazăr et al., 2019; Suk et al., 2016; Wang et al., 2021).

Prior to any *in vivo* study, a relevant preclinical investigation of each nanomedicine *in vitro* is mandatory and must be conducted using cell culture models that adequately mimic the tumor and the surrounding microenvironment, made up of cellular and acellular components (*e.g.*, extracellular matrix proteins such as fibronectin, collagen, etc…). The latter is not only involved in a key interaction with cancer cells, promoting tumor progression and aggressiveness, but also represents a solid physical barrier, the efficient crossing of which is a requirement to effectively reach the targeted cancer cells (Li and Burgess, 2020; Meng et al., 2018).

3D cell cultures are useful tools to construct *in vitro* biomimetic models capable to satisfy this need. Among the different described systems, the assembly of cells in the form of multicellular tumor spheroids (MCTS) has been widely applied for the screening of anticancer treatments (Lazzari et al., 2017; Mehta et al., 2012).

This stems from the capacity of MCTS to recreate *in vitro* some fundamental characteristics of tumor such as (i) heterogeneous cell growth, (ii) cell-to-cell crosstalk, (iii) pH, nutriments, and oxygen gradients, (iv) ECM accumulation and (v) chemoresistance. Their 3D spatial arrangement has the potential to establish the biological barriers to nanomedicines and thus allows for an efficient study of their capacity of tumor penetration and delivery of the therapeutic cargo (Alonso-Nocelo et al., 2016).

The before mentioned physical barrier acquires in pancreatic ductal adenocarcinoma (PDAC) the feature of a dense fibrotic reaction (up to 90% of the tumor mass) whose main contributors are the cancer-associated-fibroblasts (CAFs). As a whole, CAFs and desmoplasia have been recognized as a crucial factor to the poor prognosis of this disease characterized by a dramatic survival outcome, in which less than 9% of patients survive for 5 years (Latenstein et al., 2020).

In this context, we have herein reproduced the key issues of PDAC in a 3D model by timely co-culturing pancreatic cancer cells (PANC-1) and CAFs in form of MCTS. We have constructed a robust, easy to use and extremely reproducible model that has been applied to investigate the potential of biocompatible nanosystems mainly composed of sphingomyelin and vitamin E to be used for the development of novel PDAC treatments. To be noted that sphingomyelin nanosystems (SNs) have already shown the capacity to load different therapeutic cargos, including small drugs and biomolecules leading to several interesting results in biomedical applications both for drug delivery and molecular imaging (Bouzo et al., 2020; Bouzo et al.,

2021; Díez-Villares et al., 2021a; Díez-Villares et al., 2021b; Nagachinta et al., 2020a; Nagachinta et al., 2020b).

First, we have assessed the capacity of SNs to penetrate through the spheroid and cross the PDAC tumor barrier. Then, the loading of a gemcitabine (Gem) lipid prodrug derivative as a model of therapeutic payload allowed to investigate the therapeutic efficacy of the system which showed the most promising diffusion capacity.

2. Materials and Methods

2.1. Materials

DL-α-tocopherol (Vitamin E) and D-α-tocopherol polyethylene glycol 1000 succinate (TPGS), were supplied by Merck Millipore (Spain). Egg sphingomyelin (SM) was bought from Lipoid. 1,2-distearoyl-*sn*-glycero-3-phosphoethanolamine-N-[(Methoxyl polyethylene glycol)-5000] (DSPE-PEG-5k) was obtained from Nanocs (New York, USA). 4-(N)-lauroyl gemcitabine (Gem12) was bought from GalChimia S.L (A Coruña, Spain). C11 TopFluor®-Sphingomyelin (SM-TopFluor®) was provided by Avanti Polar Lipids (Alabama, USA). Gemcitabine (Gem) hydrochloride was purchased from Carbosynth Ltd. (UK). Analytical grade solvents were purchased from Sigma Aldrich (France), VWR (Spain) or Galmedic (Spain). Chemicals provided by commercial suppliers were used without additional purification. Ultrapure water was obtained with the MilliQ purification system (Merck Millipore, France).

2.2. Nanosystem formulation and characterization

Bare lipid nanosystems (SNs) were formulated as previously described (Bouzo et al., 2020; Nagachinta et al., 2020b). Briefly, opportune volumes of vitamin E (5 mg) and sphingomyelin (0.5 mg) stock solutions in ethanol were mixed and then the volume was adjusted to 100 µL with the same solvent. The resulting organic solution was injected into 900 µL of MilliQ water. An aqueous dispersion of nanosystems at a final lipid concentration of 5.5 $mg.mL^{-1}$ was immediately obtained and used without further purification. Surface-modified SNs were formulated according to the same protocol by adding TPGS (100 µg; SNs_TPGS) or DSPE-PEG-5k (100 µg; SNs_PEG) to the organic phase. For the formulation of drug-loaded SNs (SNs_Gem12), the organic phase was supplemented with 4-(N)-lauroyl gemcitabine (100 µg). Fluorescently-labeled

SNs (*denoted in the article with a* *) were formulated following the same procedure adding the SM-TopFluor® fluorescent dye (10 ng.µL^{-1}) in the ethanolic solution.

Mean diameter and size distribution (polydispersity index, PdI) of nanosystems were measured by dynamic light scattering (DLS) at 25 °C using a Zetasizer Nano ZS (Malvern Instruments, UK, 173° scattering angle). The zeta potential of nanosystems was measured using the same instrument at 25 °C after 40-fold dilution in 1 mM NaCl solution applying the Smoluchowski equation. Measurements were performed at least in triplicate.

Morphology of nanosystems was observed by Field Emission Scanning Electron Microscopy (FESEM). After filtration (0.45 µm syringe filter, Phenomenex, California, USA) samples were diluted 10 times with MilliQ water. 20 µL of the resulting dispersion was mixed with 20 µL of 2% (w/v) aqueous phosphotungstic acid solution, and 10 µL of the mixture was placed on Formvar-Carbon coated copper grids. After 2 min the excess was removed. Additional 10 µL were deposed on the grid according to the same protocol. Prepared grids were stored for 9 hours in a desiccator, washed with MilliQ water, and then finally dried in the desiccator overnight. Images were acquired using an Ultra Plus scanning electron microscope (Zeiss, Germany) operating at 20 kV configured at STEM mode.

Colloidal stability of nanosystems was investigated by monitoring mean diameter and PdI over a period of 72 h. SNs were maintained at 4 and 37 ºC (stability in water) or diluted (200x) in cell culture medium (DMEM) supplemented with 10% (v/v) fetal bovine serum (FBS) and stored at 37 °C. Mean diameter and polydispersity index were measured by DLS. Measurements were performed at least in triplicate.

2.3. *Gem12 content in sphingomyelin nanosystems*

Gem12 loading into the nanosystems was evaluated by high performance liquid chromatography (HPLC) according to a previously described method (Bastiancich et al., 2016). First, GemC12-loaded nanosystems were purified with CentriPure P10 Columns (Quimigen SL, Madrid, Spain) following the manufacturer's instructions.

Then, both purified and not-purified nanosystems were disrupted with 20-fold dilution in ethanol. Quantification of the amount of Gem12 was carried out through an HPLC system 1260 Infinity II Agilent (Agilent Technologies, US) equipped with a pump G7111A, an autosampler G7129A and an UV-Vis detector G7114A set at 248 nm. The mobile phase was composed of methanol and water (MeOH:H_2O, 90:10 v/v) at a flow rate of 1 mL.min^{-1}. Standard calibration curves were linear in the range of 0.3 to 20 µg.mL^{-1}.

The encapsulation efficiency EE (*wt %*) was determined according to the following relationship:

(1) $$EE(\%) = \frac{weight\ encapsulated\ Gem12}{weight\ added\ Gem12} x100$$

The drug loading DL (*wt%*) was determined according to the following relationship:

(2) $$DL(\%) = \frac{weight\ encapsulated\ Gem12}{weight\ lipids\ (VitE\ and\ SM) + weight\ encapsulated\ Gem12} x100$$

2.4. Cell lines

The human pancreatic cancer cell line (PANC-1) and cancer-associated-fibroblasts (CAF08) were purchased from the American Type Culture Collection (ATCC, France) and Vitro Biopharma (USA), respectively. Cells were maintained as recommended. Briefly, PANC-1 cells were cultured in Dulbecco's Modified Eagle Medium (DMEM, Sigma Aldrich, France) supplemented with 10% heat-inactivated fetal bovine serum (FBS, Gibco, France). CAF08 cells were cultured in Pancreatic Stellate CAF Maintenance medium (PC00B5, Vitro Biopharma,

USA). All media were further supplemented with penicillin (50 $U.mL^{-1}$) and streptomycin (0.05 $mg.mL^{-1}$). Cells were maintained in a humidified incubator at 37 °C and 5% CO_2. Cells were used below passage 8 after thawing.

CAF08 expression of alpha-SMA (alpha Smooth Muscle Actin), FAP (Fibroblast Activation Protein) and CD44 markers was validated by flow cytometry.

2.5. CAF08 characterization by flow cytometry

Alpha-SMA staining. Cells were harvested by trypsin and fixed with 250 µL of 4% paraformaldehyde (Roti®-Histofix 4%, Roth Sochiel EURL, France) at room temperature for 10 minutes. Cells were washed twice with PBS (200 µL), collected by centrifugation (1 500 rpm, 5 min, room temperature) and permeabilized with PBS containing 0.1% Triton X-100 (15 min, room temperature). Next, the cells were incubated for 20 min with 3% BSA to block nonspecific antibody binding. 1 x 10^6 cells were seeded into eppendorf tubes and incubated with the primary anti alpha-SMA (ab32575, Abcam, 0.25 $µg.mL^{-1}$; 1/100) or isotype (ab172730, Abcam, 0.25 $µg.mL^{-1}$) antibody in the dark for 30 min at 4°C. After incubation, the cells centrifuged (300 g, 5 min, room temperature), incubated with the secondary antibody (ab6717, 1/1000, 100 µL) in the dark for 30 min at 4°C. The cells were then washed once with PBS (100 µL), centrifuged (300 g, 5 min, room temperature), resuspended in PBS and immediately analyzed by flow cytometry (Accuri C6, BD Biosciences). Fluorescence intensities were collected in the FL1 channel (Ex 488 nm/Em 530 nm).

FAP staining. 1 x 10^6 cells were seeded in eppendorf tubes and incubated for 20 min with 3% BSA to block nonspecific antibody binding. After centrifugation (300 g, 5 min, room temperature) cells were incubated with the anti-FAP primary antibody (BMS168, Thermo Fisher, 100 µL, 3 $µg.mL^{-1}$) or isotype (IgG1 K, 14-4714-82, Thermo Fisher, 100 µL, 3 $µg.mL^{-1}$) in the

dark for 1 h at 4°C. After incubation, cells were centrifuged (300 g, 5 min, room temperature), incubated with the secondary antibody (IgG 115-545-003, Thermo Fisher, 100 µL, 1/100) in the dark for 30 min at 4°C. The cells were then washed once with PBS (100 µL), centrifuged (300 g, 5 min, room temperature), resuspended in PBS and immediately analyzed by flow cytometry (Accuri C6, BD Biosciences). Fluorescence intensities were collected in the FL1 channel.

CD44 staining. 1 x 10^5 cells were seeded in eppendorf tubes and incubated with the allophycocyanin (APC)-conjugated anti-CD44 antibody (559942, BD Biosciences, 20 µL) or isotype (555745, BD Biosciences, 20 µL) in the dark for 30 min at 4°C. After centrifugation (300 g, 5 min, room temperature) cells were washed once with PBS (100 µL), centrifuged (300 g, 5 min, room temperature), resuspended in PBS (100 µL) and immediately analyzed by flow cytometry (Accuri C6, BD Biosciences). Fluorescence intensities were collected in the FL4 channel (Ex 640 nm/Em 675 nm).

2.6 CAF08 transduction

GFP-expressing CAF08 were obtained by transduction with pLenti-C-mGFP-P2A-Puro particles (Origene, Germany) according to the manufacturer's protocol. Briefly, cells were seeded to 50% confluence in a 12-well plate (2 x 10^5 cells per well) and incubated 18-20 h at 37°C in a humidified incubator. The medium was then removed and replaced with fresh one containing lentiviral particles (transfection multiplicity 10) and polybrene (8 µg.mL^{-1}). After 24 hours, the medium containing the transducing particles was removed and replaced with fresh medium containing puromycin (0.5 µg.mL^{-1}) (Thermo Fisher, France) which was renewed every 3 days until resistant colonies were identified. Once 100% of resistant cells expressed GFP, as assessed by flow cytometry, the cells were amplified and frozen.

2.7. Assessment of nanosystem uptake by flow cytometry (2D cell culture)

PANC-1 and CAF08 cells (2.8 x 10^5 and 2 x 10^5 per well, respectively) were seeded in 12-well plates. After 24 h, media was discarded, and cells were treated with SM-TopFluor®-labeled nanosystems either bare (SNs*), or surface modified with TPGS (SNs_TPGS*) or PEG (SNs_PEG*) diluted in completed medium (final lipid concentration of 0.0275 mg.mL^{-1}) for 4 and 24 h at 37 °C. After treatment, supernatants were discarded, cells were washed with 500 µL of PBS, detached with 500 µL of trypsin and washed twice with PBS. After the last centrifugation (5 min, 200 *g*, 20 °C), the cells were resuspended in PBS before being analyzed by flow cytometry (Accuri C6, BD) and mean fluorescence intensities were collected on the FL-1 (Ex 488 nm/Em 530 nm). For each experiment, 15 000 cells per sample were measured and all experiments were performed in triplicate.

2.8. Assessment of SN uptake by CLSM (2D cell culture)

PANC-1 and CAF08 cells (2.8 x 10^5 and 2 x 10^5, respectively) were seeded in complete media onto sterile 25 mm diameter and 0.17 mm thick coverslips into a 12-well plate. After 24 h, media was discarded, and cells were treated with SM-TopFluor®-labeled nanosystems either bare (SNs*), or surface modified with TPGS (SNs_TPGS*) or PEG (SNs_PEG*) diluted in completed medium (final lipid concentration of 0.275 mg.mL^{-1}) for 4 and 24 h at 37 °C.

After treatment, cells were washed with PBS (1 mL) and then fixed with 4% paraformaldehyde (Roti®-Histofix 4%) in the dark at room temperature for 10 min. Nuclei were stained with Hoechst 33342 solution in PBS for 20 min in the dark at room temperature. Fixed cells were imaged using a confocal laser scanning microscope (CLSM, TCS SP8 gated-STED; Leica,

Germany) equipped with a CS2 Plan Apochromat 63x/NA 1.4 oil immersion objective lens and with a 405 nm diode for Hoechst excitation and a WLL laser set at 488 nm for SM-TopFluor®. Fluorescence was collected using a sequential mode, with 411-474 nm wide emission slits for the blue signal (multialkali-PMT detector) and 526-595 nm wide emission slits for the green one (Internal hybrid detector). The pinhole was set at 1.0 Airy unit. Transmission images were realized with a PMT-trans detector. Images were acquired in 1024 x 1024 pixels size, 12-bit depth, 400 Hz scanning speed using the Leica SP8 LAS X software (Version 3.5.5, Leica,Germany).

2.9. SN cytotoxicity (2D)

Assessment of cell viability after treatment with the different nanosystems was performed using the CellTiter-Glo® 2.0 assay (Promega) according to the manufacturer instructions. Briefly 100 µL of cell dispersion was seeded at different densities in a 96-well opaque plate (CLS3917, Sigma, France) (24 h treatment: 9 x 10^4 PANC-1 and 6 x 10^4 CAF08 cells *per* mL; 24 h + 48 h and 72 h treatment: 3 x 10^4 PANC-1 and 2 x 10^4 CAF08 cells *per* mL) and incubated overnight. Afterwards, cells were exposed to different concentrations of nanosystems or free gemcitabine for (i) 24 h, (ii) 24 h followed by treatment removal and 48 h culture with fresh medium without any treatment (24 h + 48 h) or (iii) 72 h at 37 °C. After treatment, a volume of CellTiter- Glo® 2.0 reagent equal to the volume of cell culture media present in each well was added (50 µL) and well content was mixed for 2 minutes on an orbital shaker. Then, plates were incubated at room temperature for 10 minutes to stabilize the luminescent signal. Luminescence measurements were performed using a benchtop plate reader (EnSpire Alpha 2390; Perkin-Elmer, USA). Cell viability was calculated as the luminescence ratio of treated versus the untreated control cells. Experiments were performed in triplicate to determine means and standard deviation.

2.10. Construction of 3D multicellular tumor spheroid (MCTS)

Heterotype MCTS made of PANC-1: CAF08 were constructed according to the liquid overlay technique (Lazzari et al., 2017) using 96 round-bottom well plates (CELLSTAR®, Sigma Aldrich, France). Before use, 50 µL of 1.2 % (w/v) ethanolic solution of poly-2-hydroxyethyl methacrylate (pHEMA, Sigma Aldrich, France) was added to each well, and the solvent was evaporated under sterile conditions. For the spheroid construction, suspensions of each cell type were prepared in DMEM complete medium supplemented with 25 $ng.mL^{-1}$ of human fibroblast growth factor (hFGF) (Sigma Aldrich, France). Then, 200 µL of their opportune mixture was transferred into each well. The number of PANC-1 cells was set at 1 000 cells *per* well. A 1:4 ratio of PANC-1: CAF08 was studied. After cell seeding, plates were centrifuged (200 *g*, 5 min, 20 °C) and then incubated in a humidified atmosphere with 5% CO_2 at 37 °C for a minimum of 72 h. For long-term culture, the medium was changed by half every 3 days. Fluorescently labeled spheroids were constructed according to the same protocol using GFP-expressing CAF08.

2.11. MCTS characterization: optical imaging

At determined time points (4, 7 and 10 days), monitoring of the constructed spheroids was performed using the AxioObserver Z1 (Carl Zeiss, Germany) inverted microscope equipped with a Peltier cooled (−40 °C) CoolSnap HQ2 CCD camera (Photometrics,Tucson, USA) and a XL incubator thermostatically controlled at 37 °C providing 5% CO_2. Transmitted light images of spheroids were acquired directly from the poly-HEMA coated plates with a Plan-Apochromat

2.5x/NA dry objective lens, a halogen lamp and a motorized stage used on an automated mode (Zen blue software/high content acquisitions).

Using an image-processing macro, specifically developed with the Image-J® software (ImageJ 1.53a, V 1.8.0), spheroid minimum and major diameter (d_1 and d_2) were measured. Spheroid volume (V) was calculated according to the formula $V = \frac{4}{3}\pi r^3$ where $r = \frac{1}{2}\sqrt{d_1 d_2}$ corresponds to the spheroid geometric mean radius. At each time point, images of 60 spheroids per condition were collected.

2.12. MCTS characterization: dissociation, single cell counting, flow cytometry analysis

At day 4, 7 and 10, six spheroids were harvested and pooled in a microtube. Culture medium was carefully removed, and spheroids were washed twice with 200 µL of PBS. Cell dissociation was performed by the action of trypsin at 37 °C for 30 min. In order to ease the dissociation of spheroids into individual cells, the cell suspension was pipetted with a p200 pipette every 5 minutes. Then, the total number of cells per sample was determined using a Kova® slide (Fisher scientific, France) and the average number of cells per spheroid was obtained by dividing by the number of spheroids used. The experiments were performed in triplicate.

Fluorescently-labeled spheroids were dissociated according to the same protocol. After centrifugation (1 500 rpm, 5 min, room temperature) cells were resuspended in PBS and analyzed by flow cytometry (Accuri C6, BD) and sorted for GFP+ cells. Experiments were performed at least in triplicate and 10 000 cells per sample were measured (Ex 488 nm/Em 530 nm).

2.13. MCTS characterization: cell viability assay

The growth of spheroids was measured over time using the CellTiter-Glo® 3D reagent, according to the manufacturer's instructions, as previously described (Lazzari et al., 2017). Briefly, 6 spheroids were collected and transferred to a microtube. After a washing step (PBS, 200 µL), the spheroids were redispersed in 50 µL of phenol red-free DMEM and transferred to white-opaque 96-well plates (Corning , Sigma Aldrich, France). To trigger spheroid lysis, 50 µL of CellTiter-Glo® 3D reagent was added to each well and the plates were kept under gentle agitation in the dark for 10 min at room temperature. The bioluminescent signal was measured after 20 min of incubation using a benchtop plate reader (EnSpire Alpha 2390, Perkin-Elmer, USA).

2.14. MCTS characterization: histology and immunohistochemistry

Spheroids were fixed for 2 h in 500 µL of 4% paraformaldehyde (Roti®-Histofix 4%, Roth Sochiel EURL, France) at room temperature. After embedding in 4% low-melting agarose (Thermo Fisher Scientific, France), spheroids were included in paraffin and cross-sectioned (Plate-Forme HistIM, Institut Cochin, Paris France). The sections (5 µm) were stained with hematoxylin and eosin (H&E) according to a standard protocol. For immunohistochemical staining, the heat-induced antigen retrieval of antibodies was performed in citrate buffer at different pH (following the manufacturer specifications) and the sections (5 µm) were then incubated with monoclonal antibody to cytokeratin AE1/AE3 (mouse, dil 1:50; M351501-2 Dako, France), or fibronectin (rabbit, dil 1:250; ab2413 Abcam, UK). Primary antibodies were detected with peroxidase-conjugated secondary antibodies by using diaminobenzidine (DAB) as chromogen and hematoxylin as a counterstain.

2.15. Assessment of SN penetration by CLSM (MCTS)

Spheroids were prepared and cultured for 4 days before incubation with SM-TopFluor®-labeled nanosystems either bare (SNs*), or surface modified with TPGS (SNs_TPGS*) or PEG (SNs_PEG*) diluted in completed medium (final lipid concentration of 0.275 mg.mL^{-1}) for 4 and 24 h at 37 °C. After treatment, spheroids were washed twice with 500 µL of PBS and fixed with 500 µL of 4% paraformaldehyde (Roti®-Histofix 4%, Roth Sochiel EURL, France) at room temperature for 1 h. Then, spheroids were permeabilized (1 h) with 500 µL of 0.1% Triton X-100 (Sigma Aldrich, France) and nuclei were stained (1 h) with Hoechst 33342 (NucBlue™ Reagent, Thermo Fisher Scientific, France) in the dark. Before imaging, spheroids were cleared accordingly to a published protocol (Dekkers et al., 2019; Pautu et al., 2021). In brief, spheroids were placed on a glass slide and, after PBS removal, covered with 100 µL of fructose/glycerol solution. After 20 min of incubation, spheroids were transferred in fresh clearing solution onto a glass slide and covered with a cover glass. Dual-sided tape was placed between the two slides to prevent the spheroids from flattening.

Images were acquired using a Confocal Laser Scanning Microscope TCS SP8 gated-STED (Leica, Germany) equipped with a HC PL APO CS2 20x/0.75 dry objective and a WLL laser with a 488 nm and a 405 nm diode with a 566-703/411-474 wide emission slits for SM-TopFluor® and Hoechst 33342, respectively. The pinhole was set at 1.0 Airy unit. Z-series optical sections were collected in 1024 x 1024 pixels size, 12-bit depth, 400 Hz scanning speed with a step of 6 µm using the LAS X software (Version 3.1.5; Leica, Germany).

SN penetration was quantified by calculating the corrected total cell fluorescence (CTCF) (Ansari et al., 2013). Spheroid contour from each stack image (14 images per spheroid, one spheroid per condition, n=3 independent experiments) was selected using the drawing tool in Fiji and area, integrated density and mean grey value were measured. The background signal was calculated

using the same protocol in untreated spheroids. The corrected total cell fluorescence was calculated according to the formula:

(3) $$CTCF = integrated\ density\ of\ the\ spheroid - (spheroid\ area * mean\ backgroundfluorescence)$$

2.16. Gemcitabine and gemcitabine-loaded SN cytotoxicity (MCTS)

Spheroids were prepared and cultured for 4 days before treatment with gemcitabine (Gem) and gemcitabine-loaded nanosystems (SN_Gem12) in complete medium at a Gem concentration of 10 and 20 µM for 24 h + 48 h or 72 h. After treatment, 150 µL of medium was removed and 50 µL of CellTiter-Glo® 3D reagent was added to each well. Plates were gently agitated in the dark for 10 min and the bioluminescence signal was measured after 20 min with a benchtop plate reader (EnSpire Alpha 2390; Perkin-Elmer, USA). Cell viability was derived as the luminescence ratio of treated to untreated spheroids.

3. Results and discussion

3.1. Nanosystem formulation and characterization.

Surface modification of nanoparticulate systems with hydrophilic PEG chains has been widely investigated to increase colloidal stability and reduce interactions with blood proteins thus endowing them with stealth and long circulating properties (Suk et al., 2016). The latter seem to be mainly conferred by long PEG chains (MW ≥ 2000), while shorter ones are described to mainly affect the interaction of nanocarriers with cells and increase the rate of internalization (Pozzi, 2014). Whether introduction of PEG chains of different length would have affected the behavior of nanosystems made of biodegradable and biocompatible lipids has been here

investigated. It is indeed well known that the ability of nanosystems to penetrate to the core of the tumors may be critical to ensure the delivery of the encapsulated drug. This is even more important in the case of the desmoplastic pancreatic tumor.

Nanosystems (SNs) made only of Vitamin E and sphingomyelin, two natural components of cell membranes, have been formulated by a simple and well reproducible injection method as previously described (Bouzo et al., 2020). Surface modification has been realized by introduction of TPGS or DSPE-PEG-5k in the organic phase before addition to the aqueous one, leading to nanosystems coated with short PEG chains (*that is*, SNs_TPGS, PEG MW 1000) or longer ones (*that is*, SNs_PEG, PEG MW 5000).

All formulated SNs showed a narrow size distribution with a negative surface charge, whose absolute value slightly decreased in presence of the PEG chains confirming their presence at the SN surface (Table 1). Compared to the other two formulations, a size reduction of around 25 nm was observed for the SNs_PEG likely due to a more pronounced effect as a surface agent of the DSPE-PEG-5k, as also previously reported (Muthu et al., 2011). Same tendency was observed for SM-Topfluor® fluorescently labeled SNs, which did not show significant differences compared to the unlabeled ones, except for SNs_TPGS in which the introduction of the dye led to a slightly more negative surface charge (Table S1).

Formulations were stable in water under storage conditions (both 4 and 37 °C) as well as in complete cell culture medium (Fig. S1, S2). The slight size increase observed for SNs_TPGS from 24 h (Fig. S1c) could be attributed to nanodroplet swelling and/or fusion but not to aggregation, as a constant value of PdI was maintained. Scanning Transmission Electron Microscopy imaging of nanosystems revealed a spherical shape and a homogeneous size distribution (Fig. 1). While the unmodified SNs exhibited fairly well-defined edges, a diffuse area

surrounded both SNs_TPGS and SNs_PEG, suggesting the presence of an effective surface coating, in a similar way than other PEGylated nanosystems (Lin et al., 2012).

Table 1: Characterization of sphingomyelin nanosystems

Formulation	Mean diameter (nm)	Polydispersity index	Zeta potential (mV)
SNs	101 ± 9	0.07 ± 0.03	-30 ± 9
SNs_TPGS	99 ± 8	0.06 ± 0.02	-8 ± 4
SNs_PEG	77 ± 3	0.06 ± 0.02	-22 ± 6

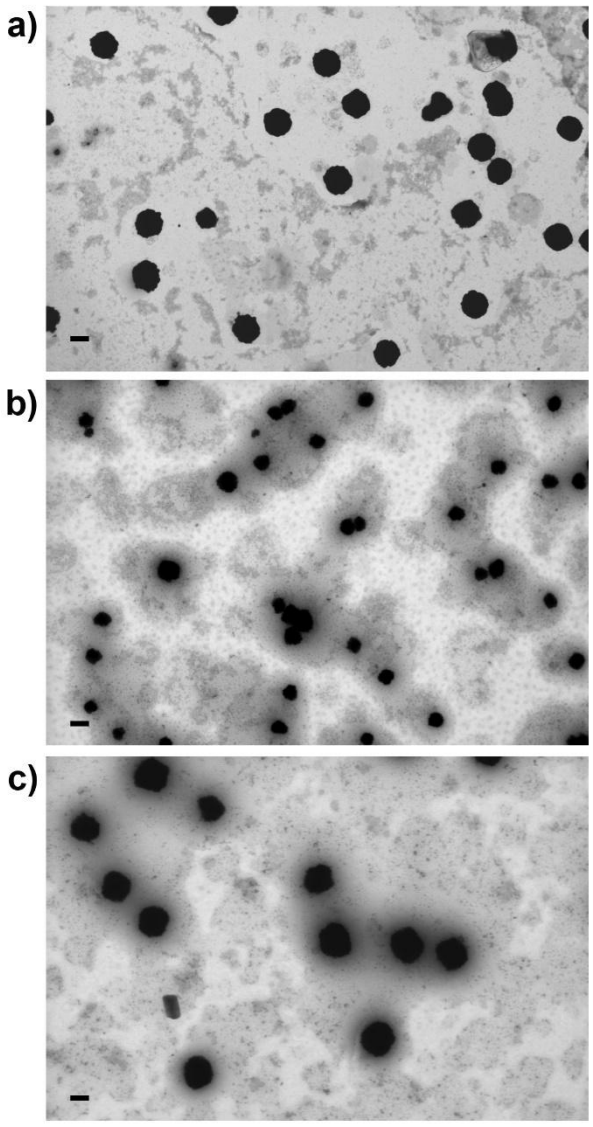

Fig. 1. Representative Scanning Transmission Electron Microscopy (STEM) images of (a) SNs, (b) SNs_TGPS, (c) SNs_PEG. Scale bars: (a) 200 nm; (b, c): 100 nm.

3.2. Construction and characterization of multicellular tumor spheroid

A model capable to mimic *in vitro* the microenvironment of PDAC has been developed by constructing heterotypic MCTS made of PANC-1 human tumor cells and CAF08 human cancer-associated-fibroblasts according to the liquid overlay technique. Although aware of the *in vivo* CAF heterogeneity (Boyd et al., 2021; Helms et al., 2020), the choice of the CAF08 cell line was motivated by its accessibility and well-defined features compared to primary cancer associated fibroblasts. Large-scale application of the latter in routine *in vitro* studies can be a challenging task due to restricted access to fresh tumor samples, lack of unique markers to identify and isolate the different subpopulations, and poorly defined culture conditions to maintain a specific phenotype over time (Han et al., 2020; Nurmik et al., 2020). The used cell line expressed characteristic CAF markers (i.e., alphaSMA, FAP and CD44) (Fig. S3).

The number of cancer cells was set at 1 000 cells *per* well at day 0, and a 1:4 PANC-1: CAF08 ratio was identified as optimal to allow the cells to spontaneously assemble in form of spheroids, without the need for any scaffolding material as well as to observe an accumulation of fibronectin a key component of the pancreatic cancer ECM, involved in tumor progression and reduction of sensitivity to treatments (Topalovski and Brekken, 2016; Vaquero et al., 2003). Regular observation by optical imaging of the spheroids revealed the formation of uniform and reproductible structures (Fig. 2a), whose size increased with time accompanied also by a gradual darkening of the central area suggesting the formation of progressively denser and thicker structure. The steady growth of spheroids was also well evidenced by the variation in spheroid volume from 0.15 ± 0.04 at day 4 to 0.48 ± 0.09 mm^3 at day 10, and the increase in the number of cells per spheroid (Fig. 2b and d). Based on the cells seeded at day 0, the total number of cells at day 4 was lower than expected as also previously observed (Lazzari et al., 2018). This further corroborated the idea that spheroid initiation required the seeding of a minimal number of cells,

but that a certain fraction is then lost over the successive hours during which cell-cell interactions increase, leading to the formation of the first compact spheroid assembly. Thereafter, spheroid growth continued consistently as confirmed by the increase in total ATP content (Fig. 2c).

As the desmoplastic reaction is well known to be involved in treatment resistance, the presence of ECM components secreted by CAF, in particular fibronectin, was investigated. Immunohistochemical staining showed a predominant compact population of cancer cells positively stained for the cytokeratin AE1/AE3 marker among which cytokeratin-negative cells were embedded and mainly accumulated in the central region. In the latter, fibronectin accumulation was observed, indicating the presence of the FN-secreting cancer associated fibroblasts (Fig. 2e-f). The presence of fibroblasts was also assessed by analysis of spheroids constructed with GFP-expressing CAF08, which confirmed their integration in the spheroid at day 4 after seeding. However, a progressive depletion of this cell population was observed over time (Fig. S4), indicating a gradual substitution by faster growing PANC-1. Such a loss has also been described previously in other models of heterotype spheroids containing fibroblasts (Lazzari et al., 2018; Eder et al., 2016; Amann et al., 2014; Kunz-Schughart et al., 2006; Eckermann et al., 2011). The integration of cells and ECM, capable to recapitulate the tumor and its microenvironment, was well observed 4 days after seeding and this was chosen as the first time point for subsequent studies.

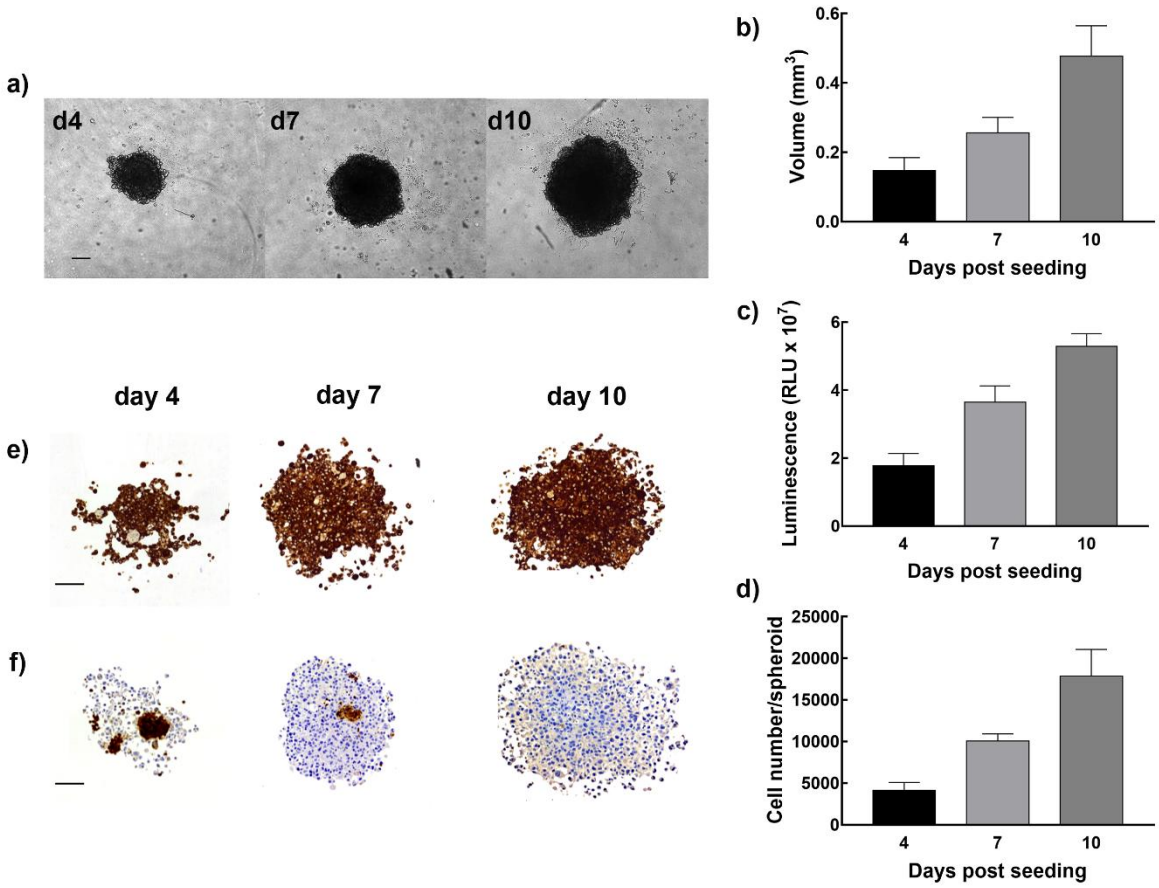

Fig. 2. Heterotype PANC-1: CAF08 characterization. (a) Representative optical imaging of spheroids (seeding density: 1 000 PANC-1 and 4 000 CAF08) at day 4, 7 and 10 post seeding. Scale bar: 200 µm. Evolution over time of spheroid (b) volume, (c) ATP content and (d) cell number. Histological analysis of 5 µm sections of tumor spheroids: (e) cytokeratin AE1/AE3 and (f) fibronectin immunostaining (brown color). Scale bars: 100 µm.

3.3. Investigation of SN in 2D cell cultures

The safety profile of the bare SNs was first validated on monolayer cultures of isolated cancer cells and cancer associated fibroblasts (Fig. S5). Exposure for 24 h to SNs at concentrations up to 0.5 $mg.mL^{-1}$ did not induce any toxicity in both cell lines. The slight increase of cell viability noticed with low concentration of SNs, could be due to either a cell stimulation and an increase in ATP content quantified in the assay or to the previously reported role of sphingomyelin in proliferation signaling pathways (Alessenko, 2000; Cutler and Mattson, 2001) as also observed for other lipid-based nanoformulations (Carmona-Ule et al., 2020). Only after 72 h incubation was a slight reduction of PANC-1 cell viability to ~75% observed (Fig. S5a). This longer treatment more adversely affected CAF08, allowing to detect a higher sensitivity of these fibroblasts compared to the cancer cells (Fig. S5b).

In order to evaluate the cell uptake of nanosystems and investigate whether the surface modification with polyethylene glycol (PEG or TPGS) would affect their capacity to be internalized by cells, PANC-1 and CAF08 were incubated with SM-TopFluor® fluorescently-labeled SNs*, SNs_TPGS* and SNs_PEG* for 4 and 24 h. Both flow cytometry and confocal microscopy showed a time dependent internalization, which was not significantly affected by the surface properties of the nanosystems (Fig. 3). While internalization extent was comparable between the two cell lines, CLSM images revealed a different intracellular distribution pattern. A diffused signal was observed in PANC-1 cells while nanosystems accumulated as green dots in CAF08 cells (Fig. 3c- d). Overall, both cell lines were capable to uptake the nanosystems and no any eventual benefit or negative effect was provided by the surface modification.

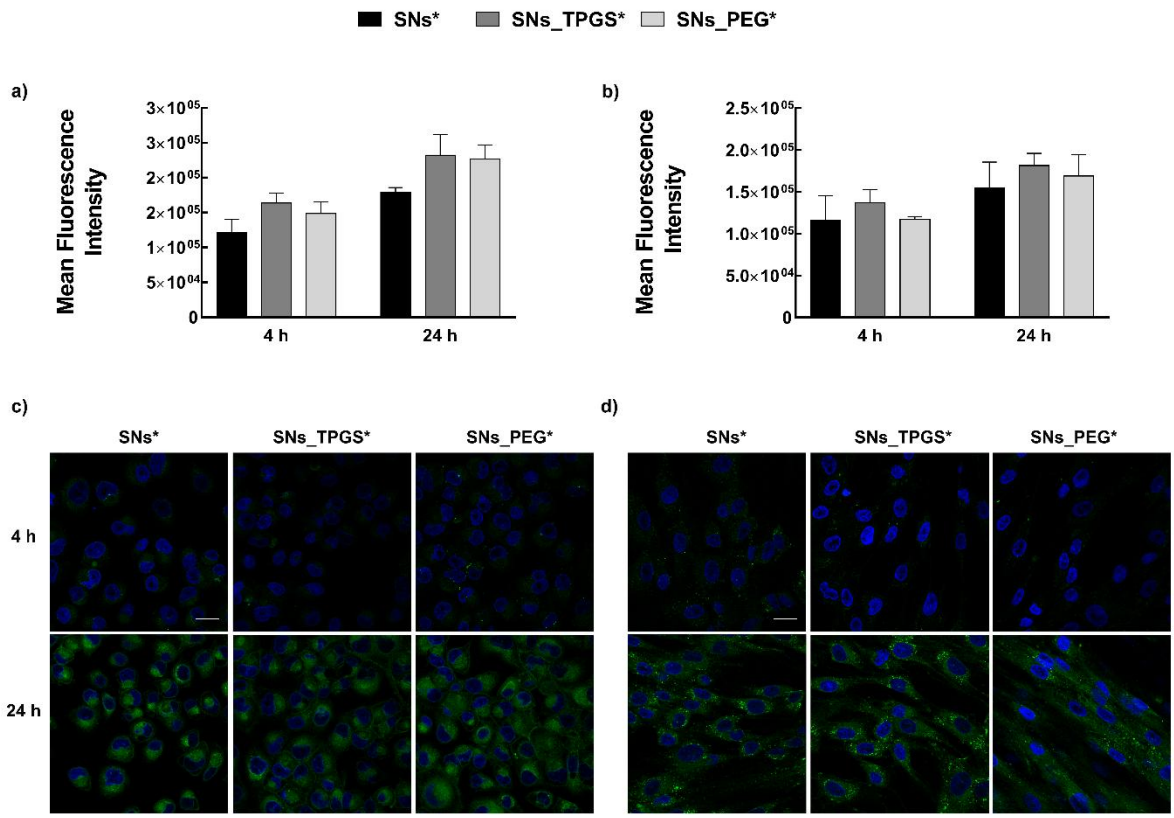

Fig. 3. Internalization of SNs*, SNs_TPGS* and SNs_PEG* in 2D cell cultures. Quantification of (a) PANC-1 and (b) CAF08 cell uptake by flow cytometry after 4 and 24 h at 37 °C. SNs were labeled with SM-TopFluor® and incubated at a final lipid concentration of 0.0275 mg.mL^{-1}. Values represent mean ± standard deviation (n=3). Confocal laser-scanning microscopy images (63x) of (c) PANC-1 and (d) CAF08 cells after incubation with fluorescently-labeled nanosystems for 4 and 24 h at 37 °C at a final lipid concentration of 0.275 mg.mL^{-1}. Merged fluorescence of blue (cell nuclei stained with Hoechst 33342) and green signal (SM-TopFluor®). Scale bars: 25 µm.

3.4. Investigation of SN penetration into MCTS by CLSM (3D cell culture)

The ability of lipid nanosystems to cross the biological barriers of tumors was evaluated in the constructed heterotype multicellular pancreatic tumor spheroid model integrating cancer cells, fibroblasts and fibronectin as a representative component of the tumor extracellular matrix. To be noted that the nanosystems did not affect the spheroid viability, even after 72 hours of incubation at the concentration of 0.55 $mg.mL^{-1}$. This permitted evaluation of their diffusion capacity without any bias that might have come from loss of structural integrity due to some cell death (Fig. S6). Imaging of clarified spheroids by CLSM after incubation with the fluorescently-labeled nanosystems well confirmed the SNs capacity to penetrate through the whole spheroid. Fluorescence pattern mainly suggested a cytosolic localization of internalized nanosystems (Fig. 4a, S7). Quantification of fluorescence intensities showed that whatever the surface properties of the SNs, no significant difference in terms of spheroid penetration and distribution could be achieved (Fig. 4b). The physico-chemical features of nanomedicines can deeply affect their capacity to cross biological barriers and efficiently deliver the loaded cargo (Blanco et al., 2015; Wilhelm et al., 2016; Lazzari et al., 2017). For instance modification of nanoparticle surface with PEG chains has been described to facilitate deeper penetration in the spheroids by decreasing the electrostatic interaction with the extracellular matrix components as well as with the cells on the surface of the spheroids (Tavares Luiz et al., 2021; Tchoryk et al., 2019; Tomasetti et al., 2016; Waite and Roth, 2012). However, given that the bare nanosystems have shown excellent capacity to cross the biological barriers in the tumor spheroid, the potential benefit associated to the presence of the hydrophilic coating has become herein negligible.

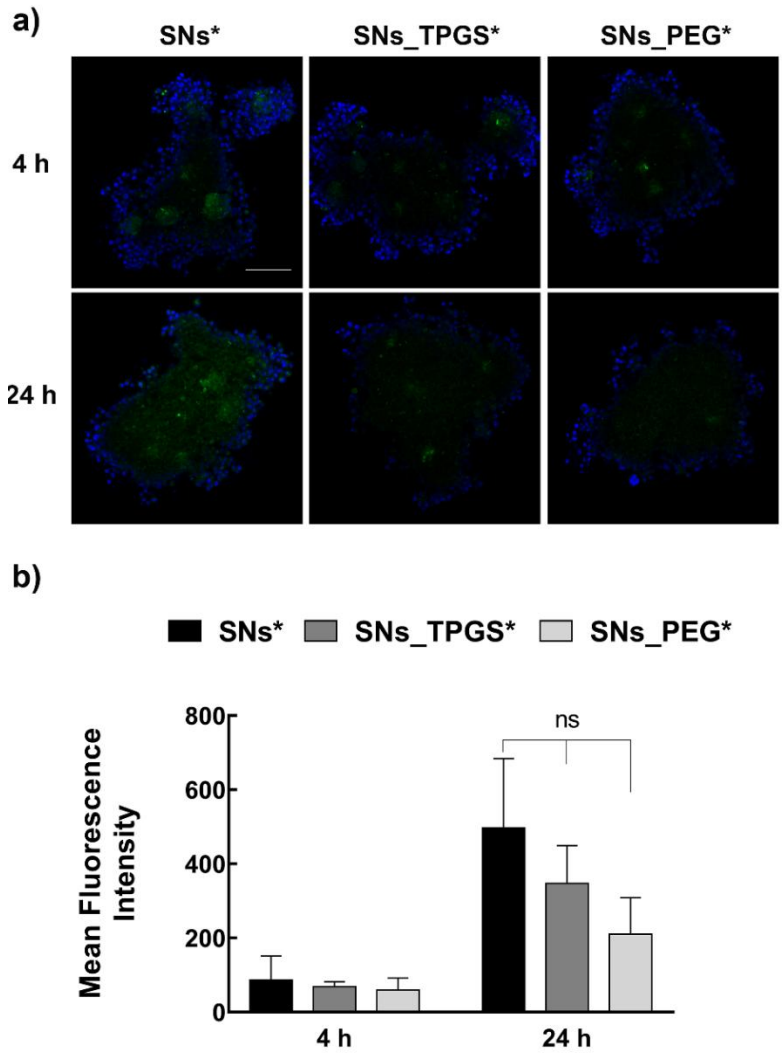

Fig. 4. Penetration of SNs*, SNs_TPGS* and SNs_PEG* in 3D tumor spheroids. (a) Confocal laser scanning microscopy imaging (20x) of spheroids treated with fluorescently-labeled nanosystems for 4 and 24 h at 37 °C at a final lipid concentration of 0.275 mg.mL^{-1}. Merged fluorescence of blue (cell nuclei stained with Hoechst 33342) and green signal (SM-TopFluor®). Images represent orthogonal section of spheroid at around 80-85 µm depth. Scale bar: 100 µm. (b) Quantification of nanosystem penetration in tumor spheroids measured at 4 and 24 h after incubation. Results are expressed as mean ± standard deviation (n=3), ns: non-significant by Kruskal-Wallis test and Dunn's multiple comparisons test.

3.5. Investigation of drug loaded SN cytotoxicity (2D culture)

According to the demonstrated effective internalization and penetration ability, and the lack of advantages brought by surface modification with the PEG chains, only the bare lipid nanosystems were selected for further studies and investigated as a suitable carrier for drug delivery. As gemcitabine (Gem) is the first line treatment in PDAC (Sloat et al., 2011), attention focused on this chemotherapeutic agent. To promote the loading of this hydrophilic drug into the lipid nanosystem a commercially available C12 derivative (Gem12) was used. It is noteworthy that not only does the hydrophobic carbon chain facilitate a better incorporation into the formulation but, being conjugated to the amino group at the 4'-position of the drug, the C12 chains also prevented the rapid metabolization of the free Gem into the inactive uracil derivative by the endogenous deaminases (Immordino et al., 2004; Moysan et al., 2014; Reddy et al., 2008). Thus, by avoiding the rapid clearance, that is one of the main limitations of this molecule, a better therapeutic activity could be achieved, as it has also been demonstrated with other gemcitabine prodrugs either as self-assembled systems or loaded in various nanocarriers (Moysan et al., 2013; Mura et al., 2015; Nagachinta et al., 2020a).

Gem12 was successfully loaded into SNs, with an entrapment efficiency of 89 ± 2.1% and a drug loading of 1.5 ± 0.1%. These gemcitabine-loaded nanosystems (SNs_Gem12) maintained a narrow size distribution (polydispersity index < 0.1), a mean diameter (98 ± 13 nm) and a negative surface charge comparable to the empty SNs (-32 ± 7 mV). SNs_Gem12 were stable in water at both 4 and 37 °C, as well as in complete cell culture medium (Fig. S8, S9).

Whether the SNs_Gem12 could provide a therapeutic advantage compared to the free drug was first investigated on 2D monolayers of PANC-1 and CAF08 cells (Fig. 5). Measurement of cell viability immediately after 24 h treatment, showed a complete absence of toxicity even at the highest concentration in both cell lines. By extending the time frame during which the activity

could be exerted, either by including a drug-free period (*i.e.*, 24 h + 48 h) or by maintaining a continuous exposure (*i.e.*, 72 h) a dose dependent toxicity was observed in PANC-1 cells. A plateau was reached with the free drug, and even after 72 h treatment at the highest concentration (*that is*, 20 μM), the percentage of viable cells was greater than 50%, clearly confirming the resistance of these cells to gemcitabine (Amrutkar and Gladhaug, 2017). However, the latter was overcome by SNs_Gem12, achieving 50% of cell death at a Gem concentration of ~ 10 μM and then increasing to ~ 65%, by doubling the drug dose (Fig. 5e). Due to the efficient uptake of the lipid nanosystems (Fig. 3), the prodrug was successfully delivered to the cancer cells, where the gemcitabine was released in a sustained manner, thereby providing better therapeutic activity compared to the free drug. These incubation schedules validated the superior therapeutic potential of SNs_Gem12 compared to the free gemcitabine also on cancer associated fibroblast (Figure 5 d,f). These cells showed higher drug sensitivity and viability was reduced to 37% ± 10% and 20.5% ± 5% after 72 h treatment at the highest concentration of Gem and SNs_Gem12, respectively (Fig. 5f).

The modest increase in cell viability observed at low, non-cytotoxic doses could, as mentioned above, be due a cell stimulation and/or promotion of proliferation triggered by sphingomyelin.

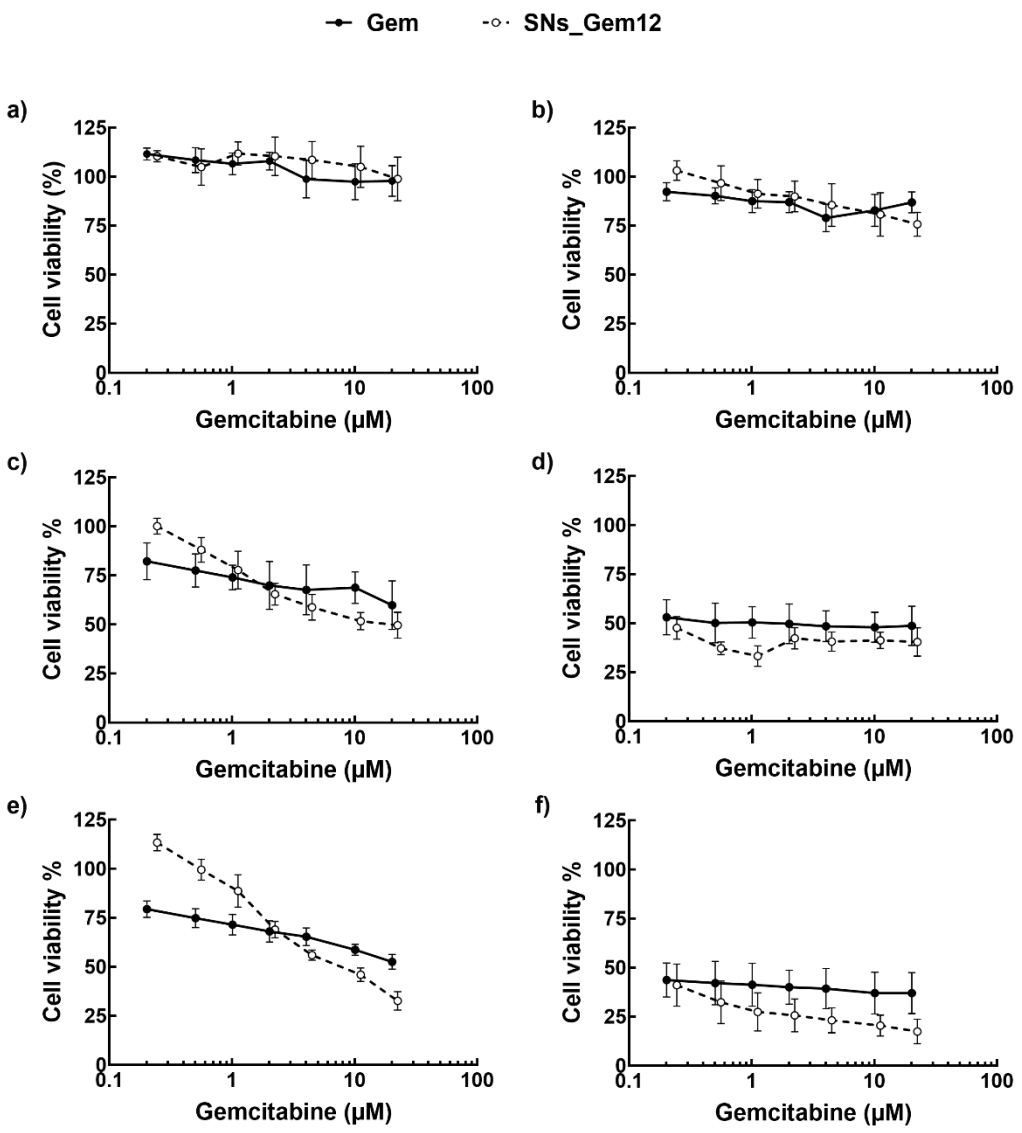

Fig. 5. Cell viability of (a, c, e) PANC-1 and (b, d, f) CAF-08 cells treated with increasing concentrations of free gemcitabine (Gem) or SNs_Gem12 for (a, b) 24 h, (c, d) 24 h + 48 h or (e, f) 72 h. Values represent mean ± standard deviation (n=3).

3.6. Investigation of drug loaded SN cytotoxicity (3D cell culture)

2D cell culture studies provided a general overview of the response (or not) of cells to treatment; however, this model remains too simplistic and does not reliably predict the effective therapeutic potential of the formulated nanosystems. Thus, further investigation was performed on the heterotype tumor spheroids, which were incubated with SNs_Gem12 or the free drug at a Gem concentration of 10 and 20 µM, chosen according with results obtained on 2D monolayers. At equivalent lipid concentration (that is, 0.275 and 0.55 $mg.mL^{-1}$) empty nanosystems did not affect viability of spheroid (Fig. S6). Only the long treatment schemes were studied based on the absence of cytotoxicity after 24 h of incubation in 2D cultures.

The resistance to the free gemcitabine evidenced in the 2D cultures was confirmed also on the MCTS. Regardless of the dose tested and incubation time, the viability of spheroids, determined by their ATP content, did not fall below 60% even after treatment with SNs_Gem12 (Fig. 6). On the contrary, exposure (72 h) of isolated PANC-1 cells cultured in 2D to SNs_Gem12 at a Gem concentration of 20 µM decreased the viability to 33% ± 5 (Fig. 5e).

Thus, while loading the prodrug into lipid nanosystems was able to provide a superior therapeutic advantage over the free drug in 2D monolayers, this benefit was lost in the 3D MCTS. Being capable to mimic some physio-pathological traits of tumors in humans, the reported superior value of the latter was acknowledged (Pozzi et al, 2021; Barbosa et al., 2021).

As we had observed the ability of lipid SNs to penetrate the spheroid, this lack of efficacy could hardly be attributed to the mere presence of the physical biological barriers of the tumor. On the contrary, the microenvironment composed of CAF and fibronectin in close communication with the cancer cells is a main attributable factor contributing to the overall higher resistance of the tumor nodule reproduced in MCTS. Indeed, a complex crosstalk between tumor cells and CAFs

leading to tumor progression, treatment resistances and metastasis has been described (Geng et al., 2021). CAFs are a major component of TME and they are considered as a key player in PDAC *via* the secretion of a large panel of cytokines, growth factors and interleukins leading to signaling pathways activation (Domen and Quatannens, 2021; von Ahrens et al., 2017). For instance, it has been reported that SDF-1/SATB-1 pathway is implicated in gemcitabine resistance (Wei et al., 2021) and numerous studies have reported the role of IL-6 in tumor cell low sensitivity to chemotherapy (Duluc et al., 2015; Zhang et al., 2015). As a result, a great interest has been oriented toward the development of effective CAF-targeted approaches (Norton et al., 2020; Sunami et al., 2021). The development of nanoformulations that allow co-delivery of combinatory therapies to simultaneously target cancer cells and CAFs could be another way of approaching.

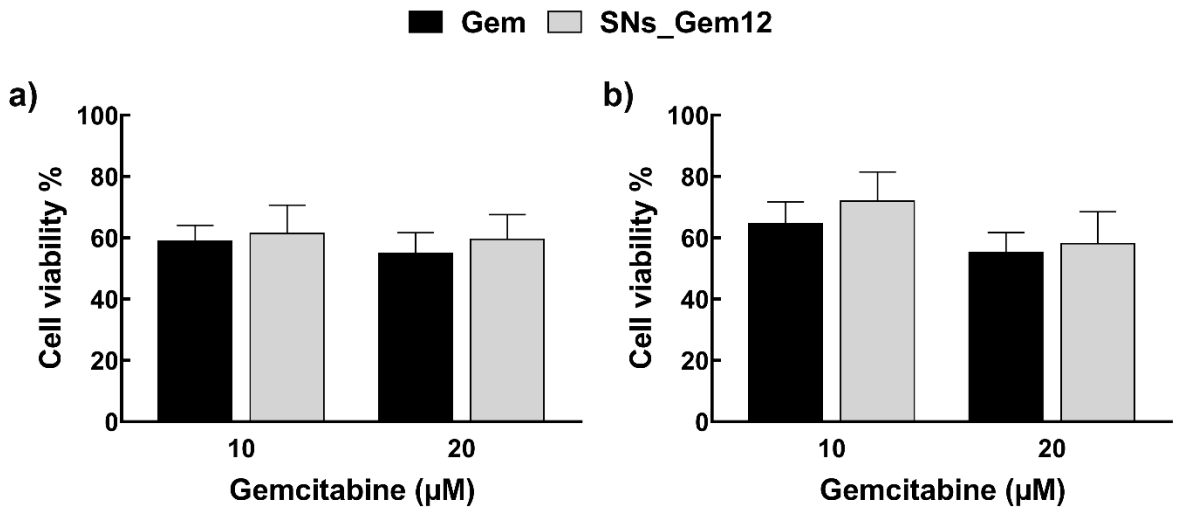

Fig. 6. PANC-1: CAF08 spheroid viability following exposure to free gemcitabine (Gem) or of SNs_Gem12 at a Gem concentration of 10 or 20 μM for (a) 24 h + 48 h or (b) 72 h. Values represent mean ± standard deviation (n=3).

4. Conclusion

Nanomedicine is a fertile field of research which holds a real potential to improve anticancer drug delivery and treatment efficiency. Although successful *in vitro* results are easily and widely claimed, failures in *in vivo* investigations are quite common and have consequently limited the number of nanomedicines that have been introduced into clinical practice. Among the various imputable factors, a major role can be attributed to the difficulty of nanomedicines of reaching the target *in vivo* due to the numerous biological barriers that characterize tumors and their microenvironment. The use of 3D tumor models is currently validated as an approach to recapitulate these features *in vitro* and to reduce the gap between the easy to use but poorly representative 2D cultures and *in vivo* studies.

In this work, biocompatible and biodegradable lipid nanosystems made of Vitamin E and Sphingomyelin have been investigated in 3D heterotype spheroids of pancreatic tumor, chosen as a model, since characterized by a dense fibrotic reaction that negatively affects the efficacy of treatments. Results clearly demonstrated the efficient capacity the nanosystems to penetrate in the tumor nodule. No advantage was conferred by introducing hydrophilic PEG chains on their surface, demonstrating that a simple system consisting of only two biocompatible components can be used as a drug carrier in ECM-rich tumors. Moreover, its simplicity would also facilitate its translation. These nanosystems were also readily loaded with the anticancer drug gemcitabine. However, despite their ability to distribute into the tumor spheroid, and their capacity to deliver

their cargo, they did not allow to achieve a significative reduction of the cell viability, likely due a higher cell resistance to the treatments in the 3D spheroid model observed also in other studies. Based on these results, it is evident that further optimization of drug-loaded lipid nanosystems would be required before moving on to preclinical *in vivo* studies in animal models.

Indeed, there are several reports of positive correlation between *in vitro* investigations of 3D tumor spheroids and *in vivo* results in experimental tumor models, highlighting the pertinence of the former for preclinical screening in the field of oncology.

For example, no significant difference was observed between paclitaxel-loaded nanodots (10 nm) and nanoparticles (70 nm) in terms of uptake and cytotoxicity on murine breast cancer cells in 2D culture. However, the nanodots were better performing in 3D spheroids as well as in an orthotopic *in vivo* model, probably due to their smaller size that promoted successful penetration and delivery of the drug, thereby inhibiting tumor progression and metastatic spread (Ni et al., 2015). Analysis of gold nanorods with different surface charges also revealed a discrepancy between the *in vitro* 2D results and those obtained in tumor spheroids. Thus, while positively charged nanoparticles exhibited the highest internalization in Hela cell monolayers, the negatively-charged ones were instead more effective in terms of penetration within both the tumor spheroids and the tumor mass *in vivo* (Sujai et al., 2020).

Similarly, the *in vitro* penetration ability, in a 3D murine breast cancer model, of nanoparticles obtained by combining doxorubicin-loaded high-chain ferritin nanocages with collagen nanocapsules, well translated into greater accumulation at the tumor site *in vivo* and inhibitory activity (Yao et al., 2020). Another example of *in vitro/in vivo* correlation with regard to drug delivery and efficacy was also described for sequentially responsive nanoparticles composed of an aptamer, a cell-penetrating peptide, and a camptothecin prodrug in a PDAC tumor model (He et al., 2020).

The ability of these lipid nanosystems to effectively penetrate through the spheroid represents a very positive starting point. Future directions to achieve higher therapeutic efficacy could include, for instance, the loading of an additional drug to exert a combination therapy on cancer cells using agents with different but complementary mechanisms of action. The development of nanosystems for the co-delivery of therapeutic agents to simultaneous target cancer cells and CAFs is another topic for future work.

Taken together, these results support the critical importance of models that closely mimic tumor features to identify candidates with the best chance of success, and thus advance promising new nanoformulations to the clinic. Noteworthy is that several improvements can still be made to 3D spheroid cultures, including the introduction of immune cell components that also play a critical role in the response to treatment and metastatic dissemination. The construction of *in vitro* 3D models using patient-derived cells is another attractive approach to predict patient response to therapy more accurately and thus enable better disease management

Acknowledgments

The research leading these results has received funding from the from Instituto de Salud Carlos III (ISCIII) and the European Regional Development Fund (FEDER) (grant number: AC18/00107) by ERA-NET EURONANOMED III project PANIPAC (grant number JTC2018/041), from Xunta de Galicia by Grupos de Potencial Crecemento (IN607B2021/14) funded by Axencia Galega de Innovación (GAIN), Consellería de Economía, Emprego e Industria. The CNRS and the French Ministry of Research are also warmly acknowledged for financial support. Saínza Lores thanks the financial support given by GAIN, Xunta de Galicia (IN606-2019/003).

Dr Delphine Courilleau, (Plate-Forme CIBLOT, Institut Paris-Saclay d'Innovation Thérapeutique, Châtenay Malabry, France) and Dr Miguel Gisbert Garzaran (Institut Galien Paris-Saclay) are warmly acknowledged for the assistance with the bioluminescence measurement. Miss Maryline Favier and miss Fabiola Ely-Marius from the HistIM Plate-Forme (Institut Cochin, Paris, France) are warmly acknowledged for their assistance with the histological analysis of spheroid samples.

Appendix A. Supplementary information

Supplementary data to this article can be found online.

References

Alessenko, A.V., 2000. The role of sphingomyelin cycle metabolites in transduction of signals of cell proliferation, differentiation and death. Membr. Cell Biol. 13, 303-320.

Alonso-Nocelo, M., Abellan-Pose, R., Vidal, A., Abal, M., Csaba, N., Alonso, M.J., Lopez-Lopez, R., de la Fuente, M., 2016. Selective interaction of PEGylated polyglutamic acid nanocapsules with cancer cells in a 3D model of a metastatic lymph node. J.Nanobiotechnology 14, 51.

Amann, A., Zwierzina, M., Gamerith, G., Bitsche. M., Huber, J.M. Vogel, G.F., Blumer, M., Koeck, S., Pechriggl, E.J., Kelm, J.M., Hilbe, W., Zwierzina H., 2014. Development of an innovative 3D cell culture system to study tumour – stroma interactions in non-small cell lung cancer cells, PLoS One 9, 3, e92511.

Amrutkar, M., Gladhaug, I.P., 2017. Pancreatic Cancer Chemoresistance to Gemcitabine. Cancers 9, 157.

Ansari, N., Müller, S., Stelzer, E., Pampaloni, F., Conn, P. M., 2013. Chapter 13 – Quantitative 3D cell-based assay performed with cellular spheroids and fluorescence microscopy. Methods in Cell Biology. 113, 295-309.

Anselmo, A.C., Mitragotri, S., 2019. Nanoparticles in the clinic: An update. Bioeng. Transl. Med. 4, e10143.

Anselmo, A.C., Mitragotri, S., 2021. Nanoparticles in the clinic: An update post COVID-19 vaccines. Bioeng. Transl. Med. e10246.

Barbosa, M., Xavier, C., Pereira, R. F., Petrikaitė, V., & Vasconcelos, M. H., 2021. 3D Cell Culture Models as Recapitulators of the Tumor Microenvironment for the Screening of Anti-Cancer Drugs. Cancers, 14, 190

Barenholz, Y., 2012. Doxil®--the first FDA-approved nano-drug: lessons learned. J. Control Release.160, 117-134.

Bastiancich, C., Vanvarenberg, K., Ucakar, B., Pitorre, M., Bastiat, G., Lagarce, F., Preat, V., Danhier, F., 2016. Lauroyl-gemcitabine-loaded lipid nanocapsule hydrogel for the treatment of glioblastoma. J. Control Release. 225, 283-293.

Blanco, E., Shen, H., Ferrari, M. 2015. Principles of nanoparticle design for overcoming biological barriers to drug delivery. Nat. Biotechnol., 33, 941–951.

Bor, G., Mat Azmi, I.D., Yaghmur, A., 2019. Nanomedicines for cancer therapy: current status, challenges and future prospects. Ther. Del. 10, 113-132.

Bouzo, B.L., Calvelo, M., Martin-Pastor, M., Garcia-Fandino, R., de la Fuente, M., 2020. In vitro-in silico modeling approach to rationally designed simple and versatile drug delivery systems. J. Phys. Chem. B 124, 5788-5800.

Bouzo, B.L., Lores, S., Jatal, R., Alijas, S., Alonso, M.J., Conejos-Sánchez, I., de la Fuente, M., 2021. Sphingomyelin nanosystems loaded with uroguanylin and etoposide for treating metastatic colorectal cancer. Sci. Rep. 11, 17213.

Boyd, L., Andini, K. D., Peters, G. J., Kazemier, G., & Giovannetti, E., 2021. Heterogeneity and plasticity of cancer-associated fibroblasts in the pancreatic tumor microenvironment. Sem. Cancer Biol. S1044-579X(21)00056-0.

Carmona-Ule, N., Abuín-Redondo, C., Costa, C., Piñeiro, R., Pereira-Veiga, T., Martínez-Pena, I., Hurtado, P., López-López, R., de la Fuente, M., Dávila-Ibáñez, A.B., 2020. Nanoemulsions to support ex vivo cell culture of breast cancer circulating tumor cells. Mater. Today Chem.16, 100265.

Cutler, R.G., Mattson, M.P., 2001. Sphingomyelin and ceramide as regulators of development and lifespan. Mech. Ageing Dev. 122, 895-908.

Dekkers, J.F., Alieva, M., Wellens, L.M., Ariese, H.C.R., Jamieson, P.R., Vonk, A.M., Amatngalim, G.D., Hu, H., Oost, K.C., Snippert, H.J.G., Beekman, J.M., Wehrens, E.J., Visvader, J.E., Clevers, H., Rios, A.C., 2019. High-resolution 3D imaging of fixed and cleared organoids. Nat. Protocols 14, 1756-1771.

Díez-Villares, S., Pellico, J., Gómez-Lado, N., Grijalvo, S., Alijas, S., Eritja, R., Herranz, F., Aguiar, P., de la Fuente, M., 2021a. Biodistribution of (68/67)ga-radiolabeled sphingolipid nanoemulsions by pet and spect imaging. Int. J. Nanomed. 16, 5923-5935.

Díez-Villares, S., Ramos-Docampo, M.A., da Silva-Candal, A., Hervella, P., Vázquez-Ríos, A.J., Dávila-Ibáñez, A.B., López-López, R., Iglesias-Rey, R., Salgueiriño, V., Fuente, M.d.l., 2021b. Manganese ferrite nanoparticles encapsulated into vitamin e/sphingomyelin nanoemulsions as contrast agents for high-sensitive magnetic resonance imaging. Adv. Healthc. Mater., 2101019.

Domen, A., Quatannens, D., 2021. Cancer-Associated Fibroblasts as a Common Orchestrator of Therapy Resistance in Lung and Pancreatic Cancer. 13, 987.

Duluc, C., Moatassim-Billah, S., Chalabi-Dchar, M., Perraud, A., Samain, R., Breibach, F., Gayral, M., Cordelier, P., Delisle, M.B., Bousquet-Dubouch, M.P., Tomasini, R., Schmid, H., Mathonnet, M., Pyronnet, S., Martineau, Y., Bousquet, C., 2015. Pharmacological targeting of the protein synthesis mTOR/4E-BP1 pathway in cancer-associated fibroblasts abrogates pancreatic tumour chemoresistance. EMBO Mol. Med. 7, 735-753.

Eckermann, C. W., Lehle, K., Schmid, S. A., Wheatley, D. N., & Kunz-Schughart, L. A., 2011. Characterization and modulation of fibroblast/endothelial cell co-cultures for the in vitro preformation of three-dimensional tubular networks. Cell Biol. Int. 35, 11, 1097-1110.

Eder, T., Weber, A., Neuwirt, H., Grünbacher, G., Ploner, C., Klocker, H., Sampson, N., Eder, I.E., 2016. Cancer-Associated Fibroblasts Modify the Response of Prostate Cancer Cells to Androgen and Anti-Androgens in Three-Dimensional Spheroid Culture. Int. J. Mol. Sci. 17, 1458.

Filipczak, N., Pan, J., Yalamarty, S.S.K., Torchilin, V.P., 2020. Recent advancements in liposome technology. Adv. Drug Deliv. Rev. 156, 4-22.

Garcia-Pinel, B., Porras-Alcala, C., Ortega-Rodriguez, A., Sarabia, F., Prados, J., Melguizo, C., Lopez-Romero, J.M., 2019. Lipid-based nanoparticles: application and recent advances in cancer treatment. Nanomaterials 9, 638.

Geng, X., Chen, H., Zhao, L., Hu, J., Yang, W., Li, G., Cheng, C., Zhao, Z., Zhang, T., Li, L., Sun, B., 2021. Cancer-associated fibroblast (CAF) heterogeneity and targeting therapy of CAFs in pancreatic cancer. Front. Cell Dev. Biol. 9, 655152.

Han, C., Liu, T. & Yin, R., 2020. Biomarkers for cancer-associated fibroblasts. Biomark. Res. 8**,** 64.

He, X., Chen, X., Liu, L., Zhang, Y., Lu, Y., Zhang, Y., Chen, Q., Ruan, C., Guo, Q., Li, C., Sun, T., & Jiang, C., 2018. Sequentially triggered nanoparticles with tumor penetration and intelligent drug release for pancreatic cancer therapy. Adv. Sci. 5, 1701070

Helms, E., Onate, M. K., & Sherman, M. H., 2020. Fibroblast Heterogeneity in the Pancreatic Tumor Microenvironment. Cancer Discov. 10, 648–656.

Immordino, M.L., Brusa, P., Rocco, F., Arpicco, S., Ceruti, M., Cattel, L., 2004. Preparation, characterization, cytotoxicity and pharmacokinetics of liposomes containing lipophilic gemcitabine prodrugs. J. Control. Release. 100, 331-346.

Kim, C.H., Lee, S.G., Kang, M.J., Lee, S., Choi, Y.W., 2017. Surface modification of lipid-based nanocarriers for cancer cell-specific drug targeting. J. Pharm. Investig. 47, 203-227.

Kunz-Schughart, L. A., Schroeder, J. A., Wondrak, M., van Rey, F., Lehle, K., Hofstaedter, F., & Wheatley, D. N., 2006. Potential of fibroblasts to regulate the formation of three-dimensional vessel-like structures from endothelial cells in vitro. Am. J. Physiol. Cell Physiol., 290, 5, C1385–C1398.

Large, D.E., Abdelmessih, R.G., Fink, E.A., Auguste, D.T., 2021. Liposome composition in drug delivery design, synthesis, characterization, and clinical application. Adv. Drug Deliv. Rev.176, 113851.

Latenstein, A.E.J., van der Geest, L.G.M., Bonsing, B.A., Groot Koerkamp, B., Haj Mohammad, N., de Hingh, I., de Meijer, V.E., Molenaar, I.Q., van Santvoort, H.C., van Tienhoven, G., Verheij, J., Vissers, P.A.J., de Vos-Geelen, J., Busch, O.R., van Eijck, C.H.J., van Laarhoven, H.W.M., Besselink, M.G., Wilmink, J.W., Dutch Pancreatic Cancer, G., 2020. Nationwide trends in incidence, treatment and survival of pancreatic ductal adenocarcinoma. Eur. J. Cancer 125, 83-93.

Layek, B., Gidwani, B., Tiwari, S., Joshi, V., Jain, V., Vyas, A., 2020. Recent Advances in Lipid-based Nanodrug Delivery Systems in Cancer Therapy. Current Pharm. Des. 26, 3218-3233.

Lazăr, L.F., Olteanu, E.D., Iuga, R., Burz, C., Achim, M., Clichici, S., Tefas, L.R., Nenu, I., Tudor, D., Baldea, I., Filip, G.A., 2019. Solid lipid nanoparticles: vital characteristics and prospective applications in cancer treatment. Crit. Rev. Ther. Drug Carrier Syst. 36, 537-581.

Lazzari, G., Couvreur, P., Mura, S., 2017. Multicellular tumor spheroids: a relevant 3D model for the in vitro preclinical investigation of polymer nanomedicines. Polym. Chem. 8, 4947-4969.

Lazzari, G., Nicolas, V., Matsusaki, M., Akashi, M., Couvreur, P., Mura, S., 2018. Multicellular spheroid based on a triple co-culture: A novel 3D model to mimic pancreatic tumor complexity. Acta Biomater. 78, 296-307.

Li, J., Burgess, D.J., 2020. Nanomedicine-based drug delivery towards tumor biological and immunological microenvironment. Acta Pharm. Sin. B 10, 2110-2124.

Lin, Y.L., Liu, Y.K., Tsai, N.M., Hsieh, J.H., Chen, C.H., Lin, C.M., Liao, K.W., 2012. A Lipo-PEG-PEI complex for encapsulating curcumin that enhances its antitumor effects on curcumin-sensitive and curcumin-resistance cells. Nanomed.: Nanotechnol. Biol. Med. 8, 318-327.

Mehta, G., Hsiao, A.Y., Ingram, M., Luker, G.D., Takayama, S., 2012. Opportunities and challenges for use of tumor spheroids as models to test drug delivery and efficacy. J. Control Release.164, 192-204.

Meng, H., Leong, W., Leong, K.W., Chen, C., Zhao, Y., 2018. Walking the line: The fate of nanomaterials at biological barriers. Biomaterials 174, 41-53.

Moysan, E., Bastiat, G., Benoit, J.-P., 2013. Gemcitabine versus Modified Gemcitabine: A Review of Several Promising Chemical Modifications. Mol. Pharm. 10, 430-444.

Moysan, E., Gonzalez-Fernandez, Y., Lautram, N., Bejaud, J., Bastiat, G., Benoit, J.P., 2014. An innovative hydrogel of gemcitabine-loaded lipid nanocapsules: when the drug is a key player of the nanomedicine structure. Soft Matter 10, 1767-1777.

Mura, S., Bui, D.T., Couvreur, P., Nicolas, J., 2015. Lipid prodrug nanocarriers in cancer therapy. J. Control Release. 208, 25-41.

Muthu, M.S., Kulkarni, S.A., Xiong, J., Feng, S.S., 2011. Vitamin E TPGS coated liposomes enhanced cellular uptake and cytotoxicity of docetaxel in brain cancer cells. Int. J. Pharm. 421, 332-340.

Nagachinta, S., Becker, G., Dammicco, S., Serrano, M.E., Leroi, N., Bahri, M.A., Plenevaux, A., Lemaire, C., Lopez, R., Luxen, A., de la Fuente, M., 2020a. Radiolabelling of lipid-based nanocarriers with fluorine-18 for in vivo tracking by PET. Colloids Surf. B Biointerfaces 188, 110793.

Nagachinta, S., Bouzo, B.L., Vazquez-Rios, A.J., Lopez, R., Fuente, M., 2020b. Sphingomyelin-Based Nanosystems (SNs) for the Development of anticancer miRNA therapeutics. Pharmaceutics 12.

Ni, D., Ding, H., Liu, S., Yue, H., Bao, Y., Wang, Z., Su, Z., Wei, W., & Ma, G., 2015. Superior intratumoral penetration of paclitaxel nanodots strengthens tumor restriction and metastasis prevention. Small, 11, 2518–2526

Norton, J., Foster, D., Chinta, M., Titan, A., Longaker, M., 2020. Pancreatic cancer associated fibroblasts (CAF): under-explored target for pancreatic cancer treatment. Cancers 12, 1347.

Nurmik, M., Ullmann, P., Rodriguez, F., Haan, S., & Letellier, E., 2020. In search of definitions: Cancer-associated fibroblasts and their markers. Int. J. Cancer, 146, 895–905.

Pautu, V., Zhao, H., Mielcarek, A., Balasso, A., Couvreur, P., Serre, C., Mura, S., 2021. When drug nanocarriers miss their target: extracellular diffusion and cell uptake are not enough to be effective. Biomater. Sci. 9, 5407-5414.

Pozzi, D., Colapicchioni, V., Caracciolo, G., Piovesana, S., Capriotti ,A.L., Palchetti,, S., De Grossi S., Riccioli, A., Amenitsch, H., Laganà, A. 2014. Effect of polyethyleneglycol (PEG) chain length on the bio-nano-interactions between PEGylated lipid nanoparticles and biological fluids: from nanostructure to uptake in cancer cells. Nanoscale 6, 2782-2792.

Pozzi, S., Scomparin, A., Israeli Dangoor, S., Rodriguez Ajamil, D., Ofek, P., Neufeld, L., Krivitsky, A., Vaskovich-Koubi, D., Kleiner, R., Dey, P., Koshrovski-Michael, S., Reisman, N., & Satchi-Fainaro, R., 2021. Meet me halfway: Are in vitro 3D cancer models on the way to replace in vivo models for nanomedicine development?. Adv. Drug Deliv. Rev 175, 113760.

Reddy, L.H., Marque, P.E., Dubernet, C., Mouelhi, S.L., Desmaele, D., Couvreur, P., 2008. Preclinical toxicology (subacute and acute) and efficacy of a new squalenoyl gemcitabine anticancer nanomedicine. J. Pharmacol. Exp. Ther. 325, 484-490.

Sloat, B.R., Sandoval, M.A., Li, D., Chung, W.G., Lansakara, P.D., Proteau, P.J., Kiguchi, K., DiGiovanni, J., Cui, Z., 2011. In vitro and in vivo anti-tumor activities of a gemcitabine derivative carried by nanoparticles. Int. J Pharm. 409, 278-288.

Suk, J.S., Xu, Q., Kim, N., Hanes, J., Ensign, L.M., 2016. PEGylation as a strategy for improving nanoparticle-based drug and gene delivery. Adv. Drug Deliv. Rev. 99, 28-51.

Sunami, Y., Boker, V., Kleeff, J., 2021. Targeting and reprograming cancer-associated fibroblasts and the tumor microenvironment in pancreatic cancer. Cancers 13.

Tavares Luiz, M., Delello Di Filippo, L., Carolina Alves, R., Sousa Araújo, V.H., Lobato Duarte, J., Maldonado Marchetti, J., Chorilli, M., 2021. The use of TPGS in drug delivery systems to overcome biological barriers. Eur. Polym. J.142, 110129.

Sujai, P. T., Joseph, M. M., Saranya, G., Nair, J. B., Murali, V. P., Maiti, K. K., 2020. Surface charge modulates the internalization vs. penetration of gold nanoparticles: comprehensive scrutiny on monolayer cancer cells, multicellular spheroids and solid tumors by SERS modality. Nanoscale, 12, 6971–6975.

Tchoryk, A., Taresco, V., Argent, R.H., Ashford, M., Gellert, P.R., Stolnik, S., Grabowska, A., Garnett, M.C., 2019. Penetration and uptake of nanoparticles in 3D tumor spheroids. Bioconjug. Chem. 30, 1371-1384.

Tibbitt, M.W., Dahlman, J.E., Langer, R., 2016. Emerging frontiers in drug delivery. JACS 138, 704-717.

Tomasetti, L., Liebl, R., Wastl, D.S., Breunig, M., 2016. Influence of PEGylation on nanoparticle mobility in different models of the extracellular matrix. Eur. J. Pharm. Biopharm.108, 145-155.

Topalovski, M., Brekken, R.A., 2016. Matrix control of pancreatic cancer: New insights into fibronectin signaling, Cancer Lett. 381, 252–258.

Vaquero, E.C., Edderkaoui, M., Nam, K.J., Gukovsky, I., Pandol, S.J., Gukovskaya, A.S., 2003. Extracellular matrix proteins protect pancreatic cancer cells from death via mitochondrial and nonmitochondrial pathways, Gastroenterology 125, 1188–1202.

von Ahrens, D., Bhagat, T.D., Nagrath, D., Maitra, A., Verma, A., 2017. The role of stromal cancer- associated fibroblasts in pancreatic cancer. Journal of hematology & oncology 10, 76.

Waite, C.L., Roth, C.M., 2012. Nanoscale drug delivery systems for enhanced drug penetration into solid tumors: current progress and opportunities. Crit. Rev. Biomed. Eng. 40, 21-41.

Wang, T., Suita, Y., Miriyala, S., Dean, J., Tapinos, N., Shen, J., 2021. Advances in lipid-based nanoparticles for cancer chemoimmunotherapy. Pharmaceutics 13.

Wei, L., Ye, H., Li, G., Lu, Y., Zhou, Q., Zheng, S., Lin, Q., Liu, Y., Li, Z., Chen, R., 2021. Correction: Cancer-associated fibroblasts promote progression and gemcitabine resistance via the SDF-1/SATB-1 pathway in pancreatic cancer. Cell death & disease 12, 232.

Wilhelm, S., Tavares, A. J., Dai, Q., Ohta, S., Audet, J., Dvorak, H. F., Chan, W. C. W., 2016. Analysis of Nanoparticle Delivery to Tumours. Nat. Rev. Mater., 1, 16014, *et al.* Analysis of nanoparticle delivery to tumours. Nat. Rev. Mater. 1**,** 16014

Yao, H., Guo, X., Zhou, H., Ren, J., Li, Y., Duan, S., Gong, X., & Du, B. (2020). Mild Acid-Responsive "Nanoenzyme Capsule" Remodeling of the Tumor Microenvironment to Increase Tumor Penetration. ACS Appl. Mater. Interfaces, 12, 20214–20227.

Zhang, H., Wu, H., Guan, J., Wang, L., Ren, X., Shi, X., Liang, Z., Liu, T., 2015. Paracrine SDF-1α signaling mediates the effects of PSCs on GEM chemoresistance through an IL-6 autocrine loop in pancreatic cancer cells. Oncotarget 6, 3085-3097.